HHS Public Access

Author manuscript

J Biomed Mater Res A. Author manuscript; available in PMC 2015 December 19.

Published in final edited form as:

J Biomed Mater Res A. 2011 September 15; 98(4): 499–508. doi:10.1002/jbm.a.33125.

Quantifying the effect of pore size and surface treatment on epidermal incorporation into percutaneously implanted sphere-templated porous biomaterials in mice

Robert A. Underwood[1], **Marcia L. Usui**[1], **Ge Zhao**[1], **Kip D. Hauch**[2], **Marc M. Takeno**[2], **Buddy D. Ratner**[2,3], **Andrew J. Marshall**[4], **Xuefeng Shi**, **John E. Olerud**[1], and **Philip Fleckman**[1]

[1]Department of Medicine/Division of Dermatology; University of Washington, Seattle, Washington, USA

[2]Department of Bioengineering; University of Washington, Seattle, Washington, USA

[3]Department of Chemical Engineering, University of Washington, Seattle, Washington, USA

[4]Healionics Inc. Seattle, Washington, USA

Abstract

The sinus between skin and a percutaneous medical device is often a portal for infection. Epidermal integration into an optimized porous biomaterial could seal this sinus. In this study we measured epithelial ingrowth into rods of sphere-templated porous poly(2-hydroxyethyl methacrylate) [poly(HEMA)] implanted percutaneously in mice. The rods contained spherical 20, 40 or 60μm pores with and without surface modification. Epithelial migration was measured 3, 7 and 14 days post-implantation utilizing immunohistochemistry for pankeratins and image analysis. Our global results showed average keratinocyte migration distances of **81**μm +/− 16.85μm (SD). Migration was shorter through 20μm pores (**69.32**μm +/− 21.73) compared to 40 and 60μm (**87.04**μm +/− 13.38 and **86.63**μm +/− 8.31 respectively). Migration was unaffected by CDI surface modification without considering factors of pore size and healing duration. Epithelial integration occurred quickly showing an average migration distance of **74.13**μm +/− 12.54 after 3 days without significant progression over time. These data show that the epidermis closes the sinus within 3 days, migrates into the biomaterial (an average of 11% of total rod diameter) and stops. This process forms an integrated epithelial collar without evidence of marsupialization or permigration.

Introduction

The interface between skin and a percutaneously implanted medical device is a critical site for device success. Insertion of a medical device through the skin results in inflammation and an open sinus that persists between the skin and foreign material. Chronic inflammation can circumvent healing and the sinus becomes a portal for microbial entry and biofilm formation, which can result in local or systemic infection.[1] The ultimate goal of these studies is to determine the characteristics of a skin/material interface that allows the implant to beneficially remain incorporated in a state of quiescent tolerance. Many previous studies have examined cutaneous incorporation into a variety of biomaterial configurations, but none have quantified epidermal ingrowth to measure the influence of precisely controlled

porosity and surface characteristics of biomaterials percutaneously implanted in mice.[2] This study focuses on epidermal incorporation as a key component of overall cutaneous barrier restoration. We describe epithelial incorporation in response to implanted sphere-templated biomaterials with a range of precise pore and inter-connecting throat sizes, with and without adhesive surface modification after 3, 7 and 14 days of healing. Barrier restoration optimized via specific biomaterial configurations could serve as a guide toward engineering device interfaces for specific purposes and efficacy.

Our premise for these studies is that precisely engineered porosity of implanted materials encourages epithelial incorporation.[3–6] In our previously published studies we have made five observations using both an *in vitro* organ culture model [3,6] and an *in vivo* mouse model.[4,5] 1) *in vitro* implantation using naturally non-adhesive poly(2-hydroxyethylmethacrylate) (polyHEMA) with pore size of 20μm and interconnecting throat sizes that are 25% of the pore diameter (5μm) prevented keratinocyte incorporation, 2) keratinocytes did incorporate, *in vitro* (6 day cultures), if the 20μm poly(HEMA) porous material was treated with 1,1′ carbonyldiimidazole (CDI) to enhance cellular and protein adhesion [3], 3) the requirement of CDI surface modification was unnecessary for keratinocyte incorporation when the pore size was increased to 40μm with an 8μm diameter throat size, 4) cutaneous integration into 90μm pores was poor, and 5) *in vivo* implantation experiments using a mouse model showed consistent epidermal incorporation using a 40 micron pore size with 16μm throat size, with or without adhesive surface modification, with healing times extending to 28 days.[4]

Based on the above observations, we hypothesize: 1) an optimal porosity in the range of 20–60μm with 40% inter-connecting throat size, 2) a biomaterial surface that promotes cellular adhesion, and 3) longer healing times would result in enhanced epidermal incorporation as measured by keratinocyte migration distance into the porous biomaterial *in vivo*. This study tests epithelial incorporation into cylindrical poly(HEMA) rods that are: 1) engineered with 20, 40 or 60μm pore diameters with 40% interconnecting throat sizes, 2) untreated, (non-adhesive surface), or treated with CDI (adhesive surface), and 3) harvested at 3, 7 and 14 days, post-implantation, in a mouse model.[4,5] This time course was selected to parallel the most active epithelial response during normal acute wound healing [7,8] and the time period of potential onset of microbial infections that may occur in a clinical setting.[1]

Poly(HEMA), as an unmodified crosslinked gel, is essentially non-adhesive for both proteins and cells, hence an advantage when used as a contact lens material.[3] With CDI modification, the surface can be made adhesive to proteins and cells and serves to mimic the natural protein retentive surface characteristics of materials such as silicone.[3] This characteristic of poly(HEMA) is ideal for this study as it allows us to separate the effect of porosity and bioadhesion on keratinocyte migration without introducing widely differing materials. We have previously demonstrated that poly(HEMA) closely approximates the natural elasticity of skin and allows excellent morphologic examination of the cutaneous/biomaterial interface. Silicone, while it may be preferable for future commercial percutaneous devices due to its mechanical properties and clinical acceptance, presents great challenges in performing histology and would reduce the accuracy of migration distance measurements.[6]

Prior to this study our morphologic examinations of cutaneous incorporation used longitudinal sections cut down the length of the biomaterial implant in order to examine both epidermal and dermal interactions with the implanted porous material. It became apparent in this study, that it would be necessary to create three-dimensional morphologic data sets via serial cross-sectioning of the cylindrical implants. The epithelial migration distances were measured from a consistently perpendicular edge of the biomaterial to ensure accuracy. This measurement method, although labor intensive, provides useful knowledge that will directly inform the design of future percutaneous medical devices, as well as raise key questions concerning the biology of keratinocyte migration into foreign materials.

After a medical device breaches the skin, there exists a complex zone that must resist microbial entry and contribute to implant stability. The information presented in this study contributes new biologic information concerning epithelial incorporation, which represents an important aspect of this multi-component barrier zone.

Material and methods

Material manufacturing

Preparation of the porous poly(HEMA) implants used for this study has been described in previous studies [9–12] with the exception that in this study, cylindrical rods, rather than square implants, were used to ensure uniform epithelial contact. Briefly, a 1.5mm biopsy tool was used to punch cylindrical rods from 1 cm thick blocks of sphere-templated porous poly(HEMA) with 20, 40 or 60μm pores and inter-connecting throats that are 40% of the pore size. Rods were untreated or the surface was modified using CDI, rinsed in acetone rather than dioxane as previously described [3,4] and stored in phosphate buffered saline.

Implantation

Animal studies were conducted with University of Washington Institutional Animal Care and Use Committee approval in compliance with the NIH Guide for the Care and Use of Laboratory Animals, January 26, 1996. Eight-week-old male C57BL/6 mice (Charles River Labs, Wilmington, MA) were housed five mice per cage prior to surgery and individually housed post-procedure in a temperature-controlled animal facility. A total of 36 mice were used for the study (4 mice per each combination of pore size, material, and time point). Each mouse was implanted with 2 rods randomized between two locations on the mouse dorsum as previously described.[4] Briefly, mice were anesthetized, dorsal skin was shaved, treated with depilatory cream (1.5 min), wiped with warm moistened gauze, and cleansed with 10% povidone-iodine followed by an alcohol wipe. A 14 gauge needle was used to pierce the skin in a through and through fashion creating two wound sites midline between the scapulae 0.5 cm apart and 1 cm posterior to the ears. The rod was placed in the lumen of the needle and the needle was withdrawn leaving the porous rod implanted through the skin with the two ends of the rod extending from the two wound sites. The second implant was placed 0.5 cm caudal to the first implant in the same fashion (Figure 1A). Animals were placed on a warming pad following surgery and allowed to recover fully from anesthesia before caging.

Tissue processing

Implants, including surrounding skin, were harvested 3, 7 and 14 days after implantation. Mice were euthanized with a lethal dose of intraperitoneal Buthanasia-D (Schering-Plough Animal Health Corp., Union, NJ). The entire region containing the two biomaterial implants was excised en block from the back of each mouse down to the level of the deep fascia. The two implants were separated using a scalpel then bisected through the midline of each implant resulting in two samples each containing one wound site. Thus, each mouse resulted in four specimens. Each specimen was embedded in O.C.T. (Sakura Finetek Inc., Torrance, CA) oriented with the rod in an upright position, frozen in a slush of alcohol/dry ice and stored at −70ºC for subsequent cryosectioning (Figure 1B). The tissue orientation allowed cryosectioning to begin from the original midline of the implant. Each cryosection slide series extended from the region of dermal incorporation, adjacent to midline, through the region of epithelial incorporation extending as far toward the exit site as could be successfully sectioned (Figure 1C). Eight micron thick serial cryosections were collected alternating between two sets of microscope slides in a fashion that discarded every other cryosection. Each microscope slide contained four sections representing a tissue depth or Z-distance of 128μm and a Z-distance between individual sections of 32μm. An average of 12 slides per specimen, representing approximately 1.5mm of depth, were required to safely include the region of epidermal incorporation. This created two nearly identical sets of slide series (offset by 16μm) and a total data set of 12,000 serial sections to be used for subsequent keratinocyte immunolabeling, photomicrography and analysis.

Immunohistochemistry

Sections were immunolabeled using routine immunoperoxidase methods as previously described.[4] Primary antibodies used for marking keratinocytes were a pooled combination of rabbit anti-pankeratin (Dako, Carpenteria, CA) and rabbit anti-mouse keratin 14 (Covance, Princeton, NJ) both used at 1:1000 dilution. Secondary antibody was biotinylated goat anti-rabbit (Vector Laboratories, Burlingame, CA) used at a 1:300 dilution followed by strept-avidin-biotin complex (Vectastain Elite ABC peroxidase kit) used at 1:50 dilution, (Vector Laboratories, Burlingame, CA), and 0.12% 3,3′-diaminobenzidine (DAB) used as chromogen. Glycergel (Dako, Carpenteria, CA) was used as mounting media.

Light microscopy

Immunohistochemically labeled tissue sections were viewed using a Nikon Microphot-SA microscope utilizing a Photometrics Sensys monochrome digital camera for brightfield image capture (Figure 2A-C). Images were stored as grayscale tiff files and opened using Photoshop® CS2 (Adobe Systems Inc., San Jose, CA) with Fovea Pro® 4.0 image processing plug-ins (Reindeer Graphics Inc, Asheville NC) for image processing and analysis. Voxblast (VayTek Inc, Fairfield, IA) was used to create 3D representations and rotations of post-analyzed z-series image stacks.

Image analysis

Measuring the migrating front of keratinocyte migration was accomplished using a computer-assisted modification of a radial cell migration methodology as described by

Vernon and colleagues.[13,14] Images were opened in Photoshop®, the circular region of biomaterial was traced (Figure 2D, green mask), the center of the biomaterial was located (centroid), a series of radial lines was created emanating from the centroid at a spacing of 6º (Figure 2D), the keratin DAB stain represented by the darker pixel values in the image was thresholded in a manner creating a contour line around the region of peroxidase stain. Each intersection of a radial line and keratinocyte contour within the region of incorporation was marked on the side closest to the centroid (leading edge of migration). Single pixels or small pixel clusters that did not form a contour line with an open lumen were excluded as potential image artifacts. Lateral edges of the region of incorporation were also excluded from measurement. A Euclidean distance map was created from the region occupied by the biomaterial in which pixel value starting from the outer edge of the material were valued at 256 and the next adjacent pixel moving toward the centroid as 255 and so on. Thus the migration distance is represented in the resulting pixel value of each marked intersection between a radial line and the leading edge of the immunohistochemically determined contour. Each pixel in the calibrated image represents 3.5μm. This number was used to convert pixel values to migration distances (μm) from the biomaterial edge (Figure 2E insert). Both average and maximal migration distances were calculated. Average migration distance was used as the most stable value for determining significance while the maximal migrating front was defined as the average 2.5% of maximal distances for each grouping. This afforded the best indicator of the migrating front distance with reasonable reduction of noise.

Statistical analysis

A univariate 3-way analysis of variance (ANOVA) with split-plot design was applied to the averaged migration distance data, with pore size, material and implant duration as the three main factor effects. Dependent on findings of significance within these fixed effects, F-tests were performed to evaluate second and third order tests of effect slices or groupings. Subsequent to observed significance within these results, the final phase, using t-tests of multiple comparisons using least square means, were conducted to elucidate the specific relationships among the factors of pore size, material and time point. P-values less than 0.05 were considered to be significant. Statistical analyses were conducted using SAS 9.0 (SAS, Cary, NC).

Results

Tight contact between epidermis and biomaterial, without suggestion of open sinuses, was observed in all specimens. The average keratinocyte migration distance into the porous material as well as the average distance of the maximal migrating front (defined here as the 2.5% furthest migration distances) is summarized in Table 1. We determined, through a series of calculations comparing averages of 1% through 10% furthest distances for each grouping, that the maxima migrating fronts showed the same trend as the overall averaged data (data not shown). For example, both the overall average migration distance and the averaged 2.5% maxima migrating front distance for the 20μm porous materials are shorter than 40 and 60μm porous materials.

Figure 3 summarizes the averaged measurements of keratinocyte migration into implanted material in chart form juxtaposed to a histogram distribution of distance measurements for each grouping.

The global 3-way ANOVA analysis, F-tests for dual factors and F-tests for the separate main factors of pore size, material and healing time are summarized in Table 2. P-values less than 0.05 are shown in bold type and were considered significant.

The significant P-values, reported above (Table 2), required further statistical investigation of factor effects using F-tests of second and third order "slices". Figure 4 shows, in line chart form, these 2nd and 3rd order interactive effects on keratinocyte migration into the porous material.

Finally, t-tests of multiple comparisons showing the specific relationships exhibiting significant P-values are summarized into four conditions (Table 3).

Permigration in which the porous material would continue to fill with keratinocytes and expel the implant through normal epidermal differentiation [15] was not seen in this study. We also saw no indication of marsupialization in which the epidermis continues to grow down along side the implant with eventual expulsion. On the contrary, keratinocyte activation/ migration occurred in less than 3 days, resulting in epithelial integration that proceeded to an average depth of 81μm into the porous material and stopped. This mechanism formed an integrated epithelial "collar" or seal around the implanted device. This collar could be visualized by reconstructing the analyzed images into a three dimensional volume shown here as a stereo pair (Figure 5).

Discussion

Enhanced incorporation of skin, gingival, and bone into porous biomaterial is well documented[16–18], reviewed in Fleckman 2008[2], and optimal pore sizes have been proposed[16,19,20]. However, this study is the first quantitative assessment of pore size and surface treatment for *in vivo* epithelial incorporation into a biomaterial. In this study we show that epidermal incorporation into sphere-templated porous biomaterial occurs quickly, does not vary over the time points studied, exhibits significantly enhanced integration using pore sizes greater than 20μm and is minimally influenced by surface treatment.

While our previous *in vitro* observations showed that 20μm pores with approximately 5μm (25%) throats inhibited all keratinocyte migration[3], 20μm pores with 8μm throats, as used in this experiment, encouraged keratinocyte ingrowth whether or not the material surface was modified to promote adhesion. However, we note that the 20μm pore/8μm throat combination remains less suitable for keratinocyte migration than 40μm pores with 16μm throats. Previous studies indicated that 40μm pore size significantly enhanced dermal vascularization in a subcutaneous implantation model.[21] This, with the current data, showing no difference between 40 and 60μm pore sizes, would suggest 40μm as an optimal pore size for percutaneous applications in which both epidermal and dermal incorporation is desired. The fact that keratinocytes could migrate through a 20μm pore with 4–5μm throat only if the surface was modified to increase its surface adhesiveness [3] supports the hypothesis that

traction forces may occur between the material and keratinocyte cell surfaces, perhaps via adhesion structures such as focal adhesions or hemidesmosomes. The current observation that equal migration distances are seen using larger pore/throat sizes, despite differences in material surface chemistry, suggests that porosity functions independent of surface chemistry in promoting keratinocyte incorporation. These results indicate that the inherent surface adhesive quality of materials that can be used in a medical device, such as silicone, may not be necessary, but does not inhibit cutaneous incorporation. In our laboratory we have implanted porous silicone rods percutaneously in mice and confirmed similar epidermal incorporation (data not shown).

Healing time reveals perhaps the most utilitarian aspect of this study. Our expectation was to see a progressive increase in migration distance with little or no epidermal ingrowth at 3 days and maximum ingrowth at 14 days. The fact that no difference was seen in keratinocyte migration distance using time as a factor indicates a more rapid onset of keratinocyte activation/migration than expected and an unexpected truncation of migration. We find it interesting that this less than 3-day activation/migration coincides with healing of acute incisional wounds supporting our experimental design as an *in vivo* wound healing event.[7,8] However, the relatively short overall migration distance seen with all experimental parameters, is contrary to normal wound healing. During normal wound healing, epithelial migration can cover distances of many millimeters toward eventual wound closure. On the contrary, keratinocytes formed an integrated epithelial “collar” within 3 days with limited ingrowth and downgrowth.

From the standpoint of keratinocyte biology during wound healing, the truncation of keratinocyte migration fosters speculation concerning the mechanism or existence of stop signals. One idea is that other cell types present within the pores may influence keratinocyte migration. Our previous study identified many of these cell types as leukocytes including monocyte/macrophages, granulocytes (neutrophils) and lymphocytes.[4] Furthermore, we showed that leukocytes invade early and persist in occupying the pores. We observed keratinocytes positioning themselves in close associations with a variety of cell types rather than associating with extracellular matrix, as is seen in normal wound healing after the inflammatory stage subsides[4]. To highlight connectivity between keratinocytes and leukocytes, we point to one component of early wound healing that influences both keratinocyte migration and macrophage recruitment/maturation. Activated macrophage stimulating protein (MSP) is a protein expressed in the early phase of wound healing. MSP influences recruitment, maturation and behavioral changes in macrophages via the RON tyrosine kinase receptor. This same receptor is present and upregulated on keratinocytes post wounding. Ligation of mature MSP to the RON receptor on keratinocytes may, via a signaling cascade, cause translocation of the alpha 6, beta 4 integrin from stable adhesion structures (hemidesmosomes) to the leading edge lamellipodia of a polarized, migrating keratinocyte.[22] This event could be part of a unified wound response that accounts for both the early epithelial migration into the porous material and the presence of phenotypically distinct macrophages. On the other hand, an antagonistic effect on keratinocyte migration could be contributed to the prolonged presence of neutrophils. It has been shown that neutrophils can be detrimental to re-epithelialization in wound healing studies[23] and, when

in close proximity to keratinocytes, may lead to degradation of basement membrane proteins keratinocytes require for migration.[24]

The epidermis can, at times, extend as a sheath along the exterior portion of the implant and immunolabeling for keratin can be viewed in the pores within this portion of the biomaterial (data not shown). It is important to note that our method of sectioning from the dermal incorporation region toward the site of epidermal ingrowth resulted in a consistent measure of the basal most aspect of the zone of epidermal incorporation. This basal aspect of incorporation represents the closest correlate to the basal aspect of the migrating epithelial tongue during normal acute wound healing.

Due to changes in keratin expression that keratinocytes can undergo during wound healing, it was important to pool the two primary antibodies of pankeratin and keratin 14. We determined through prior tests that the pankeratin antibody, while excellent at marking keratinocytes in normal skin, poorly marked activated keratinocytes that were within the epithelial migrating tongue. On the other hand, staining for keratin 14 was increased within this region post-wounding.[25] This pooling insured that the entire keratinocyte migrating front could be identified regardless of the state of activation.

Sectioning became more difficult and eventually became impossible within the exit site external to viable tissue. The poly(HEMA), when not surrounded by tissue, tends to desiccate and become brittle, making cryosectioning difficult to impossible. This resulted in incomplete 3D reconstructions of the zone of epithelial incorporation (note the missing part of the collar in Figure 5). However, while the serial section data suffered from gaps within this region, the remaining data were robust enough to appreciate that the epithelial collar continued to surround and incorporate into the biomaterial. Overall, the ability to observe the histologic sections above and below the section being analyzed facilitated both the visualization of the epithelial “collar” and the accuracy of keratinocyte migration measurements.

The statistical analysis proceeded in four stages. Conducting each subsequent stage of analysis was dependent on observing P-values < 0.05 in the previous stage. As long as significant P-values were observed, analysis continued to the final stage of multiple comparisons. The global 3-way statistical analysis showed that there was, indeed, an interactive effect on keratinocyte migration among our three factors of interest, pore size, material and healing time. F-tests for dual factors showed an interaction existing between material and healing time followed by F-tests for each main factor revealing that pore size exhibited a significant effect. Data slicing and multiple comparisons revealed multiple combinations of factors that significantly influenced migration (Figure 4 and Table 2). The complexity of these multiple effects is simplified by focusing on two groups, material and 20μm pores. Using material as our factor of interest shows that migration was greatest at 7 days compared to 3 and 14 day in poly(HEMA), while CDI modification enhanced migration at 14 days compared to 14 day poly(HEMA). Using pore size as our factor of interest we see that all effects, however complex, become evident using a pore size of 20μm. Eliminating the 20μm pore size from our experiment would remove 80% of our significant findings. This would indicate that as pore size decreases there is a threshold at which

environmental variables such as material surface characteristics and healing time can exert greater influence on migration.

While acknowledging that the statistical analysis indicated probable effects of pore size or material surface over time, it is important to maintain a perspective concerning statistical vs. biological significance. The total averaged migration distance represents less than 11% of the available distance across the implanted material. The average migration range, taking into account all effects on migration distance, represents less than 42% of the total averaged migration distance or approximately 34μm of deviation. This represents a total averaged effect on migration distance of less than the distance of 2 pores in the 20μm material and less than one pore for the 40 and 60μm materials. None-the-less, our hypothesis that an optimal pore size within the range of 20–60μm will enhance keratinocyte migration into the material was upheld. Pore sizes greater than 20μm slightly enhance keratinocyte migration and abate most of the effects of material and time. Our second hypothesis stating a more adherent material surface would promote increased keratinocyte migration was also upheld to a limited degree. A slight increase in epidermal incorporation was observed in the CDI modified poly(HEMA) at day 14 ($P=0.0467$) and a more pronounced effect combining 20μm with CDI treatment at day 14 ($P=0.0007$). Our third hypothesis that keratinocyte migration distance would increase as a function of healing time was rejected. We saw no difference in migration distance comparing 3, 7 and 14 day healing times. Considering our results as a whole, we conclude that reducing the pore size to 20μm produces a biologically significant reduction in keratinocyte incorporation with increased variability.

The overarching goal associated with cutaneous interactions with biomaterials was to achieve a state of quiescent healing after which the foreign material can beneficially remain incorporated. The normal process of wound healing results in the restoration of quiescent barrier function. After implantation, healing can be separated into three phases. First is physical closure through wound healing, second is restoration of barrier function to exclude microbial invasion and third is to achieve a state of quiescent tolerance. Achieving each of these goals after implanting a foreign material through the skin could look strikingly different compared to normal wound healing. These differences have not been explored fully. Keratinocytes display a wide range of phenotypes including quiescence, active migration, signaling interactions and phagocytosis in response to wounding.[26] A keratinocyte that is attached quiescently to the biomaterial surface via slow cycling hemidesmosomes and basement membrane components may respond very differently to a microbial challenge than one that is in a perpetual state of activation. It will be important to understand what cellular phenotypic changes occur in response to percutaneously implanted biomaterials and if these changes are conducive or detrimental to each barrier function. We have shown in this study that keratinocytes migrate into cylindrical porous biomaterials at the interface between skin and biomaterial forming an incorporated collar. Currently, it is unclear if this epithelial collar sufficiently restores cutaneous quiescence in a wound healing sense, or functions as a barrier to infection. Comparative biology of the wound healing processes must be studied and microbial barrier function must be tested by challenging the biomaterial/skin interface with appropriate organisms that naturally reside on mouse skin.[27] These studies are now in progress.

This implantation model allows us to explore the phenotypic changes that occur in both keratinocytes and leukocytes to begin investigating the complex interactive biology of the barrier zone as a wound healing scenario. All components, epidermal, dermal and inflammatory, are important contributors to the healing and functionality of this barrier region and each step toward understanding the interactive biology could help guide the engineering of more effective percutaneous medical devices for a variety of applications.

Acknowledgments

This study was supported by: NIH EB 004422, The George F. Odland Endowed Research Fund and The Marvin and Judy Young Research Fund.

We express our gratitude to Dr. Zarry Tavakkol for her assistance during preliminary studies and Dr. Karen Holbrook for championing the role of morphology in pursuing our curiosities.

References

1. Safdar N, Kluger DM, Maki DG. A review of risk factors for catheter-related bloodstream infection caused by percutaneously inserted, noncuffed central venous catheters: implications for preventive strategies. Medicine (Baltimore). 2002; 81(6):466–479. [PubMed: 12441903]
2. Fleckman P, Olerud JE. Models for the histologic study of the skin interface with percutaneous biomaterials. Biomed Mater. 2008; 3(3):034006. [PubMed: 18708704]
3. Fukano Y, Knowles NG, Usui ML, Underwood RA, Hauch KD, Marshall AJ, Ratner BD, Giachelli C, Carter WG, Fleckman P, et al. Characterization of an in vitro model for evaluating the interface between skin and percutaneous biomaterials. Wound Repair Regen. 2006; 14(4):484–491. [PubMed: 16939578]
4. Fukano Y, Usui ML, Underwood RA, Isenhath S, Marshall AJ, Hauch KD, Ratner BD, Olerud JE, Fleckman P. Epidermal and dermal integration into sphere-templated porous poly(2-hydroxyethyl methacrylate) implants in mice. J Biomed Mater Res A. 94(4):1172–1186. [PubMed: 20694984]
5. Isenhath SN, Fukano Y, Usui ML, Underwood RA, Irvin CA, Marshall AJ, Hauch KD, Ratner BD, Fleckman P, Olerud JE. A mouse model to evaluate the interface between skin and a percutaneous device. J Biomed Mater Res A. 2007; 83(4):915–922. [PubMed: 17567856]
6. Knowles NG, Miyashita Y, Usui ML, Marshall AJ, Pirrone A, Hauch KD, Ratner BD, Underwood RA, Fleckman P, Olerud JE. A model for studying epithelial attachment and morphology at the interface between skin and percutaneous devices. J Biomed Mater Res A. 2005; 74(3):482–488. [PubMed: 15983994]
7. Odland G, Ross R. Human wound repair. I. Epidermal regeneration. J Cell Biol. 1968; 39(1):135–151. [PubMed: 5678445]
8. Olerud JE, Gown AM, Bickenbach J, Dale B, Odland GF. An assessment of human epidermal repair in elderly normal subjects using immunohistochemical methods. J Invest Dermatol. 1988; 90(6): 845–850. [PubMed: 2453586]
9. Marshall, AJ. PhD dissertation. University of Washington; 2004. Porous hydrogels with well-defined pore structure for biomaterials applications.
10. Marshall AJ, Ratner BD. A new technique for fabrication of macroporous hydogels. Transactions of the Society for Biomaterials. 2001
11. Marshall, AJ.; Ratner, BD. Porous hydogel scaffolds for tissue engineering. 2002.
12. Marshall AJ, Ratner BD. Quantitative characterization of sphere-templated porous biomaterials. AIChE Journal. 2005; 51(4):1221–1232.
13. Vernon RB, Gooden MD. New technologies in vitro for analysis of cell movement on or within collagen gels. Matrix Biol. 2002; 21(8):661–669. [PubMed: 12524052]
14. Vernon RB, Sage EH. A novel, quantitative model for study of endothelial cell migration and sprout formation within three-dimensional collagen matrices. Microvasc Res. 1999; 57(2):118–133. [PubMed: 10049660]

15. von Recum AF. Applications and failure modes of percutaneous devices: a review. J Biomed Mater Res. 1984; 18(4):323–336. [PubMed: 6234317]
16. Winter GD. Transcutaneous implants: reactions of the skin-implant interface. J Biomed Mater Res. 1974; 8(3):99–113. [PubMed: 4616966]
17. Von Recum AF, Park JB. Permanent percutaneous devices. CRC Crit Rev Bioeng. 1981; 5(1):37–77.
18. Fitton JH, Dalton BA, Beumer G, Johnson G, Griesser HJ, Steele JG. Surface topography can interfere with epithelial tissue migration. J Biomed Mater Res. 1998; 42(2):245–257. [PubMed: 9773820]
19. Yannas IV, Lee E, Orgill DP, Skrabut EM, Murphy GF. Synthesis and characterization of a model extracellular matrix that induces partial regeneration of adult mammalian skin. Proc Natl Acad Sci U S A. 1989; 86(3):933–937. [PubMed: 2915988]
20. Murphy CM, Haugh MG, O'Brien FJ. The effect of mean pore size on cell attachment, proliferation and migration in collagen-glycosaminoglycan scaffolds for bone tissue engineering. Biomaterials. 31(3):461–466. [PubMed: 19819008]
21. Marshall AJ, Irvin CA, Barker T, Sage EH, Hauch KD, Ratner BD. Biomaterials with tightly controlled pore size that promote vascular in-growth. Polym Preprints. 2004; 45:100–101.
22. Santoro MM, Gaudino G, Marchisio PC. The MSP receptor regulates alpha6beta4 and alpha3beta1 integrins via 14-3-3 proteins in keratinocyte migration. Dev Cell. 2003; 5(2):257–271. [PubMed: 12919677]
23. Dovi JV, Szpaderska AM, DiPietro LA. Neutrophil function in the healing wound: adding insult to injury? Thromb Haemost. 2004; 92(2):275–280. [PubMed: 15269822]
24. Briggaman RA, Schechter NM, Fraki J, Lazarus GS. Degradation of the epidermal-dermal junction by proteolytic enzymes from human skin and human polymorphonuclear leukocytes. J Exp Med. 1984; 160(4):1027–1042. [PubMed: 6384417]
25. Usui ML, Underwood RA, Mansbridge JN, Muffley LA, Carter WG, Olerud JE. Morphological evidence for the role of suprabasal keratinocytes in wound reepithelialization. Wound Repair Regen. 2005; 13(5):468–479. [PubMed: 16176455]
26. Underwood RA, Carter WG, Usui ML, Olerud JE. Ultrastructural localization of integrin subunits beta4 and alpha3 within the migrating epithelial tongue of in vivo human wounds. J Histochem Cytochem. 2009; 57(2):123–142. [PubMed: 18824633]
27. Tavakkol Z, Samuelson D, Delancey Pulcini E, Underwood RA, Usui ML, Costerton JW, James GA, Olerud JE, Fleckman P. Resident Bacterial Flora in the Skin of C57BL/6 Mice Housed under SPF Conditions. J Am Assoc Lab Anim Sci. 49(5):588–591. [PubMed: 20858360]

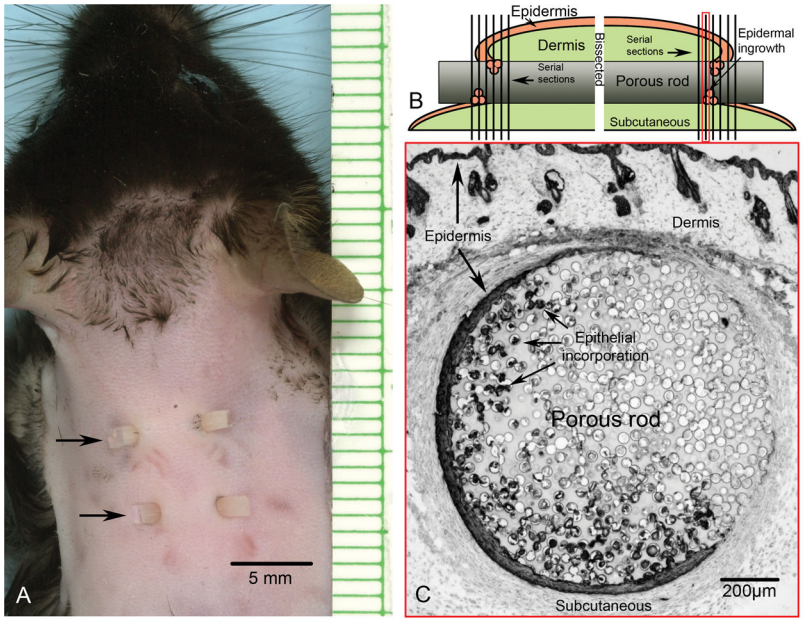

Figure 1.

A) Mouse implantation model showing two porous cylindrical rods (arrows) using a through and through method creating four sites of epidermal/biomaterial contact. B) Illustration depicting a longitudinal view through one implant. Each implant was bisected perpendicular to the long rod axis of the implant and serially crossectioned starting from the interior region. Sectioning progressed through the region of epidermal incorporation and ended toward the exit site. C) Representative photomicrograph within the region of epidermal incorporation, as indicated by a red border (1B), after immunohistochemical labeling for keratin showing the circular crossection of a rod with 40μm pores and surrounding cutaneous tissue, 7 days post-implantation. The epidermis migrates a distance down along the rod prior to the region of incorporation. Thus, in crossection, the epidermal incorporation is not contiguous, nor does it always appear closest to the outer epidermis that bridges dorsally over the implant. Epidermis adjacent to the rod appears as a separate island until becoming contiguous toward the exit site.

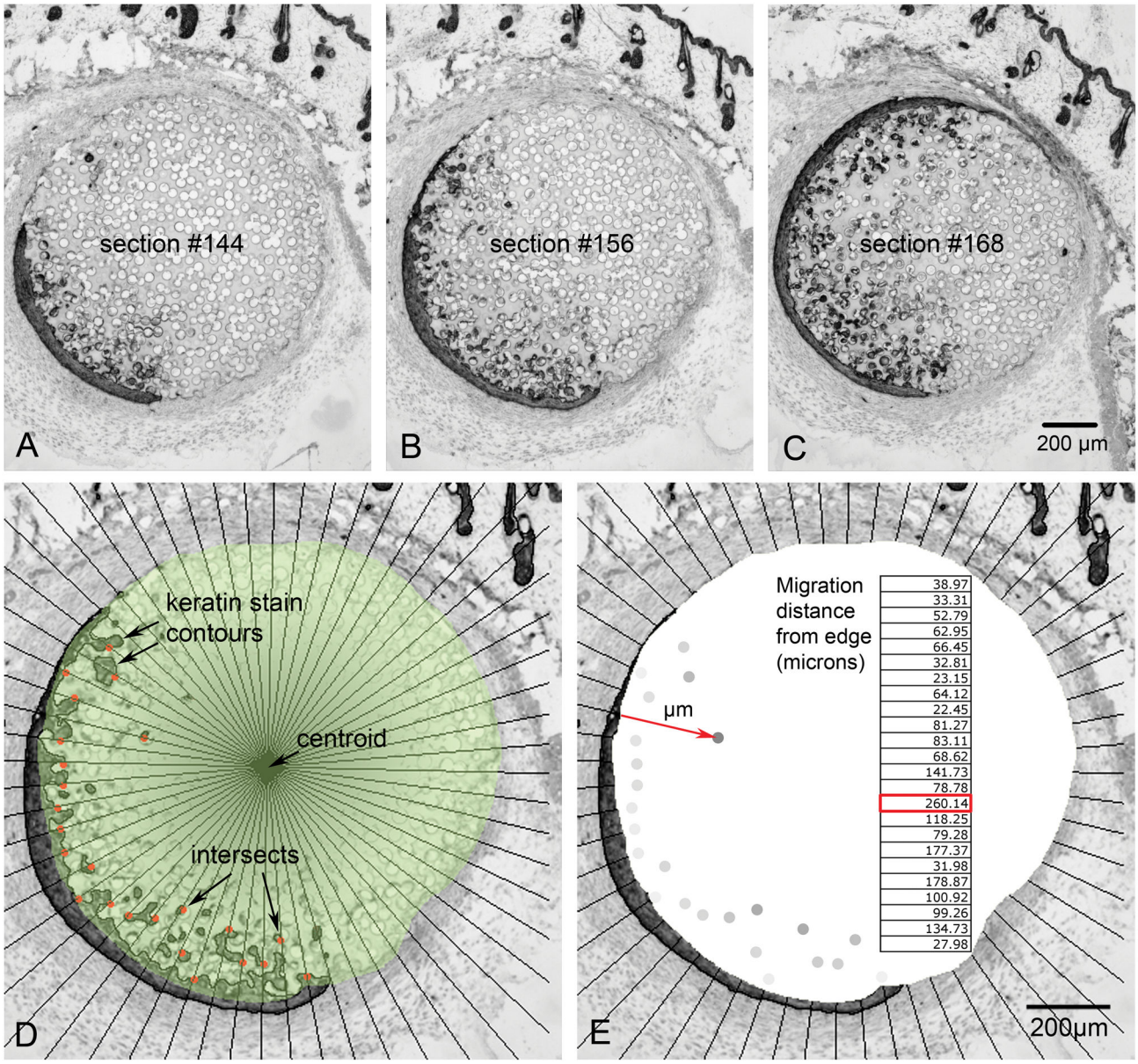

Figure 2.

A, B, C) This partial sequence of photomicrographs, spaced at 96μm intervals in the Z-direction, demonstrates epithelial incorporation into the 40μm pores of poly(HEMA) 7 days after implantation. D) Analyzed photomicrograph shows radial lines emanating from the centroid (central arrow) of the biomaterial (green mask), the contours outlining the keratin stain and intersects between radial lines and contours nearest the centroid (red dots). E) Same micrograph as D, showing how the Euclidean distance map assigned pixel values to each intersect according to its distance from the biomaterial's edge (red arrow). Using image calibration, the pixel values were converted to microns (embedded table).

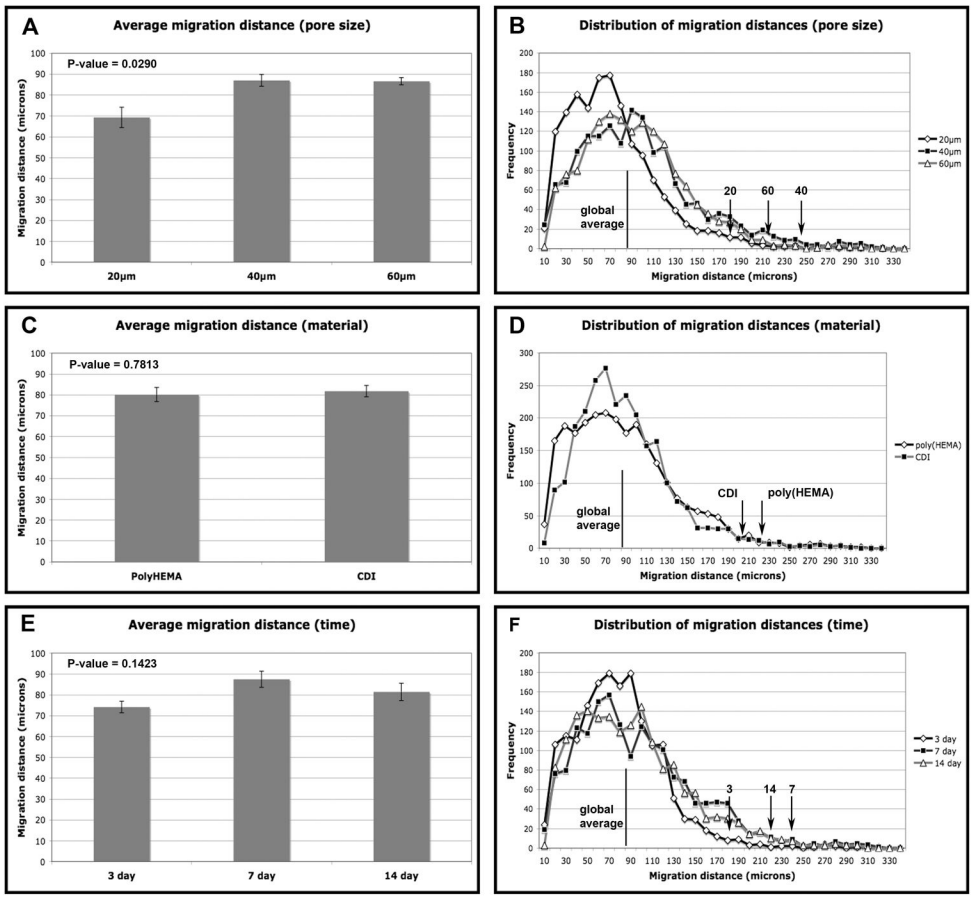

Figure 3.

A) Charted data comparing the average migration distance grouped into 20, 40 and 60µm pores sizes regardless of material treatment or healing time. B) Distribution of migration distances for 20, 40 and 60µm pore sizes (midline indicates global average and arrows indicate positions of the migrating fronts for each pore size). C) Charted data comparing the average migration distance of poly(HEMA) and CDI modified poly(HEMA) regardless of pore size or healing time. D) Distribution of migration distances for poly(HEMA) and CDI (midline indicates global average and arrows indicate positions of the migrating fronts for each material). E) Charted data comparing the average migration distance of 3, 7 and 14 days of healing time regardless of pore size and material treatment. F) Distribution of migration distances for 3, 7 and 14 days of healing time (midline indicates overall average and arrows indicate positions of the averaged 2.5% furthest distances, or maximal front, for each healing time). Error bars represent standard error. P-values less than 0.05 are considered significant.

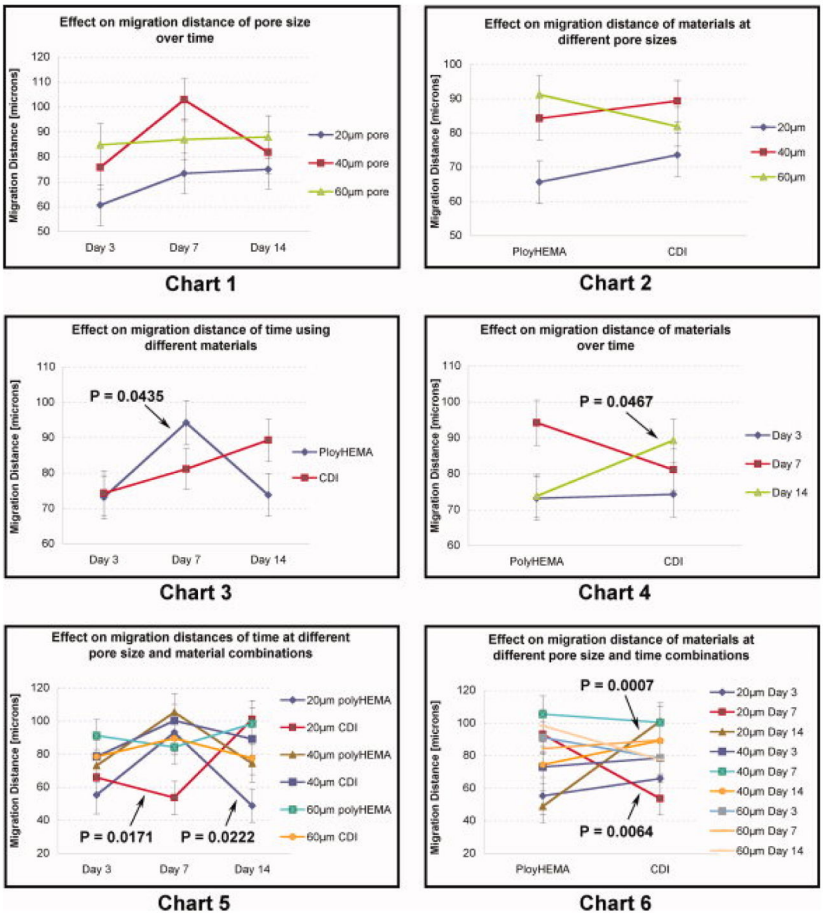

Figure 4.

Chart 1) Line chart compares the effect on migration distance that 20, 40 or 60µm pore sizes exhibit over time. Chart 2) Line chart shows the effect that poly(HEMA) or CDI modified poly(HEMA) material has comparing rods with 20, 40 or 60µm pore sizes. Chart 3) Line chart shows the effect on migration distance of poly(HEMA) and CDI modified poly(HEMA) over time. Chart 4) Line chart shows the effect on migration distance of healing time of 3, 7 and 14 days comparing poly(HEMA) and CDI modified poly(HEMA). Chart 5) Line chart shows the effect on migration distance of pore size/material combinations over time. Chart 6) Line chart shows the effect on migration distance of pore size/time combinations comparing poly(HEMA) and CDI modified poly(HEMA). Error bars depict standard error and P values less than 0.05 are indicated by arrows.

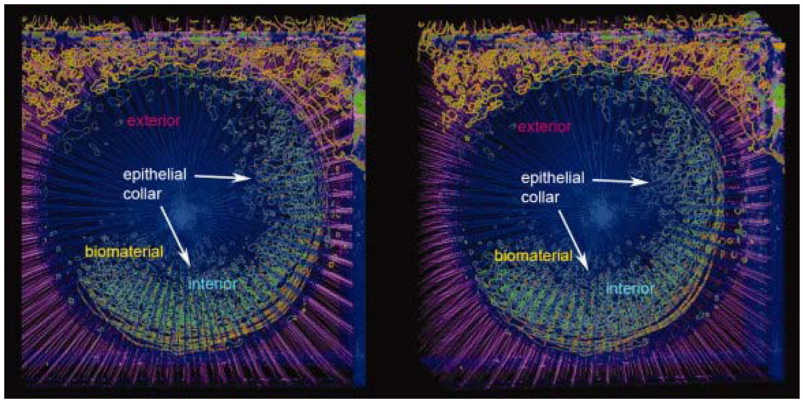

Figure 5.

Stereo pair representing the 3D reconstruction of analyzed micrographs through the region of epithelial incorporation as viewed from the ventral aspect. Green depicts the contours surrounding keratin stain within the porous biomaterial. Keratin stain contours (hair follicles and epidermis) outside the biomaterial are depicted in orange. Red dots depict the intersection between radial lines and keratinocyte stain contours and represent the epithelial migrating front. Radial lines within the biomaterial are represented in blue while radial lines outside the biomaterial are magenta.

Table 1

Average migration distances

Summary of averaged migration distances and the 2.5% maximal migration front distances. Groupings are shown in row 1. Average distances and corresponding standard deviation and error are shown in row 3 and 4 respectively. The 2.5% averaged furthest distances, or maximal migrating front and their corresponding standard deviation and error values is shown in rows 6 and 7.

Grouping	Average distance	SD	SEM	Averaged migrating front	SD	SEM
All	81.00	16.85	3.97	208.21	57.90	23.63
20μm	69.32	21.73	4.86	175.64	67.29	27.47
40μm	87.04	13.38	2.85	239.58	55.04	22.47
60μm	86.63	8.31	1.73	209.39	37.24	15.20
Poly(HEMA)	80.16	19.09	3.37	218.16	58.69	23.96
CDI	81.83	15.41	2.72	198.26	58.81	24.00
3 day	74.13	12.54	2.74	176.31	56.10	22.90
7 day	87.45	18.11	3.86	234.38	56.85	23.04
14 day	81.41	19.32	4.12	213.93	54.21	22.13

Table 2

Global ANOVA Tests of Fixed Effects

Results using a univariant 3-way statistical analysis (ANOVA) with split plot design.
Row 1: Shows a significant interactive effect of pore size, material and healing time. Rows 2–4: Shows the global ANOVA F-test results for the dual factors of pore/material, pore/time and material/time. The dual factors of material/time show a significant interactive effect. Rows 5–7: shows ANOVA F-tests for each main factor of pore size, material and healing time. Pore size showed a statistically significant effect.

Factors	P-value
1) Pore*Material*time	**0.0035**
2) Pore*Material	0.2103
3) Pore*time	0.4917
4) Material*time	**0.0404**
5) Pore	**0.0290**
6) Material	0.7813
7) Time	0.1423

Table 3

t-tests of Multiple Comparisons (P<0.05)

Results showing t-tests of multiple comparisons.

Summarized data shows the specific relationships that were found to be statistically significant.

Row 1) Keratinocytes within 40μm and 60μm pores migrated further compared with 20μm pores. Row 2) 20μm poly(HEMA) at 7 days migrated further than 20μm poly(HEMA) at both 3 days and 14 days. Row 3) 20μm CDI modified poly(HEMA) at 14 days migrated further than 20μm CDI at 3 and 7 days. Row 4) poly(HEMA) at 7 days migrated further than poly(HEMA) at 3 days and 14 days.

Effect/Grouping	P-values < 0.05
1) Migration through 40 and 60μm is greater than 20μm	**P=0.0200/0.0189 respectively**
2) 20μm poly(HEMA), 7 day > 20μm poly(HEMA), 3 and 14 day	**P=0.0303/0.0089 respectively**
3) 20μm CDI, 14 day > 20μm CDI, 3 and 7 day	**P=0.0417/0.0056 respectively**
4) Poly(HEMA), 7 day > poly(HEMA), 3 and 14 day	**P=0.0261/0.0303 respectively**